

PAPER • OPEN ACCESS

## Time stability and connectivity analysis with an intracortical 96-channel microelectrode array inserted in human visual cortex

To cite this article: Fabrizio Grani *et al* 2022 *J. Neural Eng.* **19** 045001

View the [article online](#) for updates and enhancements.

You may also like

- [Monogamy and trade-off relations for correlated quantum coherence](#)  
Marcos L W Basso and Jonas Maziero
- [Enhancement of EEG–EMG coupling detection using corticomuscular coherence with spatial–temporal optimization](#)  
Jingyao Sun, Tianyu Jia, Zhibin Li et al.
- [Curvature-enhanced multipartite coherence in the multiverse](#)  
Shu-Min Wu, , Chun-Xu Wang et al.



## PAPER

## OPEN ACCESS

RECEIVED  
3 January 2022REVISED  
5 July 2022ACCEPTED FOR PUBLICATION  
11 July 2022PUBLISHED  
22 July 2022

Original content from  
this work may be used  
under the terms of the  
[Creative Commons  
Attribution 4.0 licence](#).

Any further distribution  
of this work must  
maintain attribution to  
the author(s) and the title  
of the work, journal  
citation and DOI.



# Time stability and connectivity analysis with an intracortical 96-channel microelectrode array inserted in human visual cortex

Fabrizio Grani<sup>1</sup> , Cristina Soto-Sanchez<sup>1</sup> , Fernando Daniel Farfan<sup>2</sup> , Arantxa Alfaro<sup>1</sup> ,  
Maria Dolores Grima<sup>1</sup> , Alfonso Rodil Doblado<sup>1</sup> and Eduardo Fernández<sup>1,\*</sup>

<sup>1</sup> Bioengineering Institute, University Miguel Hernández, Elche, Spain

<sup>2</sup> Departamento de Bioingeniería Facultad de Ciencias Exactas y Tecnología, Universidad Nacional de Tucumán, Tucumán, Argentina

\* Author to whom any correspondence should be addressed.

E-mail: [e.fernandez@umh.es](mailto:e.fernandez@umh.es)

**Keywords:** neuroprosthesis, brain plasticity, long-term measurements

Supplementary material for this article is available [online](#)

## Abstract

**Objective.** Microstimulation via electrodes that penetrate the visual cortex creates visual perceptions called phosphenes. Besides providing electrical stimulation to induce perceptions, each electrode can be used to record the brain signals from the cortex region under the electrode which contains brain state information. Since the future visual prosthesis interfaces will be implanted chronically in the visual cortex of blind people, it is important to study the long-term stability of the signals acquired from the electrodes. Here, we studied the changes over time and the repercussions of electrical stimulation on the brain signals acquired with an intracortical 96-channel microelectrode array implanted in the visual cortex of a blind volunteer for 6 months. **Approach.** We used variance, power spectral density, correlation, coherence, and phase coherence to study the brain signals acquired in resting condition before and after the administration of electrical stimulation during a period of 6 months. **Main results.** Variance and power spectral density up to 750 Hz do not show any significant trend in the 6 months, but correlation coherence and phase coherence significantly decrease over the implantation time and increase after electrical stimulation. **Significance.** The stability of variance and power spectral density in time is important for long-term clinical applications based on the intracortical signals collected by the electrodes. The decreasing trends of correlation, coherence, and phase coherence might be related to plasticity changes in the visual cortex due to electrical microstimulation.

## 1. Introduction

Microelectrode arrays, such as the Utah electrode array (UEA) which contains 100 penetrating microneedles, have been widely used to record and stimulate different brain areas [1–3]. The neural signals collected with UAEs inserted in the motor cortex have been successfully used to build brain–machine interfaces that decode motor intention and are able to control robotic platforms [4–8]; and in combination with functional electrical stimulation to control body parts in tetraplegic patients [9–11]. Furthermore, UAEs might form the foundation for the restoration of a useful visual sense in the blind [12, 13] and contribute to a better understanding of visual information processing in the brain [14]. In addition, it has

been recently demonstrated that recorded activity with UEA in a visual brain area (V4), can be used to predict thresholds for phosphenes perception when the primary visual cortex is stimulated [15], which suggests that a closed-loop approach could help to improve the performance, safety and long-term stability of electrical stimulation in the brain.

The signals collected with UEA can be divided into two categories: local field potentials (LFPs, frequency smaller than 400 Hz) and action potentials (multi-unit activity or single-unit activity, high-frequency signals). LFPs are the result of the summation of voltage changes generated by the neural activity in the surrounding of the electrode [16–18]. The synchronized activity of surrounding neurons produces oscillations in the LFP signal [19]. The

frequency of these oscillations provides insights into cognitive activity and brain state [20]. Likewise, the signals recorded through UEA provide specific information about local neural networks [21, 22], source locations of specific components of visual evoked potentials [23], and brain plasticity [24].

With the aim of building a permanent visual prosthesis, it is important to understand how the brain tissue reacts to the insertion of the electrodes, the stability of the decoding accuracy with time, and the stability of LFPs signals recorded with UAEs [25]. Moreover, neuronal recordings can also provide information about the possible deleterious effects of chronic intracortical microstimulation on the electrode–tissue interface [26, 27]. Thus, the long-term characterization of aspects such as time stability, and connectivity analysis of action potentials and LFPs is of seminal relevance in this field. These kinds of studies are scarce, especially in humans, and to the best of our knowledge have not been performed in the primary visual cortex of a blind subject.

Sharma *et al* [28] described the trend of signals acquired from a UEA inserted in the motor cortex of a macaque over a 7.5 months period. They showed that the power spectral density at frequencies lower than 1000 Hz does not change with time while at frequencies higher than 1000 Hz it decreases with time due to a reduction in the number of recorded action potentials. On the other hand, Kellis *et al* [29] described the signals recorded from a UEA inserted in human motor cortex in terms of synchronization between LFPs acquired by the different electrodes using correlation, coherence, and phase coherence. However, these results were limited to a 10 min intraoperative measure, which does not give insights into how these measures could change in a chronically implanted device.

In this study, we implanted an intracortical 96-channels array (UEA) in the primary visual cortex of a blind subject and performed electrical stimulation and neural recordings over a period of 6 months. We consistently obtained LFP recordings from visually deprived populations of neurons and evaluated measures that describe single channel features in time and frequency (variance and power spectral density), as well as channels synchronization in time (correlation), frequency (coherence), and phase (phase coherence). Our results show that the recorded signals remained consistently stable over time. The synchronization between channels is higher immediately after electrical stimulation, and it decreases over the 6 months, which could be related to plastic changes in response to intracortical microstimulation.

## 2. Methods

### 2.1. Implant and recordings

The methods are described in greater detail in a previous paper [30] and are only summarized here.

An intracortical microelectrode array consisting of 96 microelectrodes (UEA) has been implanted in the visual cortex of a 57 years old person with complete blindness for the last 16 years, during a period of 6 months (figure 1(a)). Reference and ground electrodes were uninsulated platinum wires and they were positioned in the brain tissue, near the implanted UEA. Procedures were approved by the Hospital General Universitario de Elche Clinical Research Committee and registered at ClinicalTrials.gov (NCT02983370). The participant gave consent to participate in the experiments which were conducted in accordance with recognized standards.

Electrical stimulation and neural recordings sessions were generally performed 5 d per week (Monday to Friday) for up to 4 h per session (the timeline of recording days in the 6 months is depicted in figure 1(b)) and each experimental session was preceded and concluded by a 1–2 min period of spontaneous neural recordings (figure 1(c)). The length of stimulation experiments varied from day to day, but no delay occurred between the before stimulation recording and the stimulation experiments, and between the stimulation experiments and the after stimulation recording. Before starting a recording, we always asked the participant to relax and be comfortable, and we only started the recordings when she was ready.

Current stimulation was delivered using a Ceres-tim 96 multichannel microstimulation system (Blackrock Microsystems Inc., Salt Lake City, UT) and customized software was used to deliver multiple stimulation patterns to different subsets of electrodes. Neural recordings were acquired using the NeuroPort data acquisition system (Blackrock Microsystems Inc., Salt Lake City, UT). Data were sampled at 30 kHz. The analogue signals were amplified and filtered (1st order high-pass at 0.3 Hz and 3rd order low-pass at 7500 Hz) with the line noise cancellation filter at 50 Hz. No other hardware filters were applied.

In this work, the 96 channels spontaneous signals acquired before and after stimulation protocols during the 6 months of the clinical trial have been studied in terms of variance and power spectral density to check the signals' stability during the 6 months, and in terms of correlation, coherence, and phase coherence to evaluate the network synchronization and connectivity. Although high-quality recordings were obtained from the day after the surgery, we included in the analysis only the recordings acquired at the university, after the volunteer was dismissed by the hospital to maintain uniformity in the recording conditions. The experiments were very simple in the initial sessions and increased with complexity over time. In the first months, the task was based on single/group electrodes stimulation followed by the answer of the participant about the perception experience. Once the distinction between spontaneous and induced phosphenes was clear, the stimulation experiments

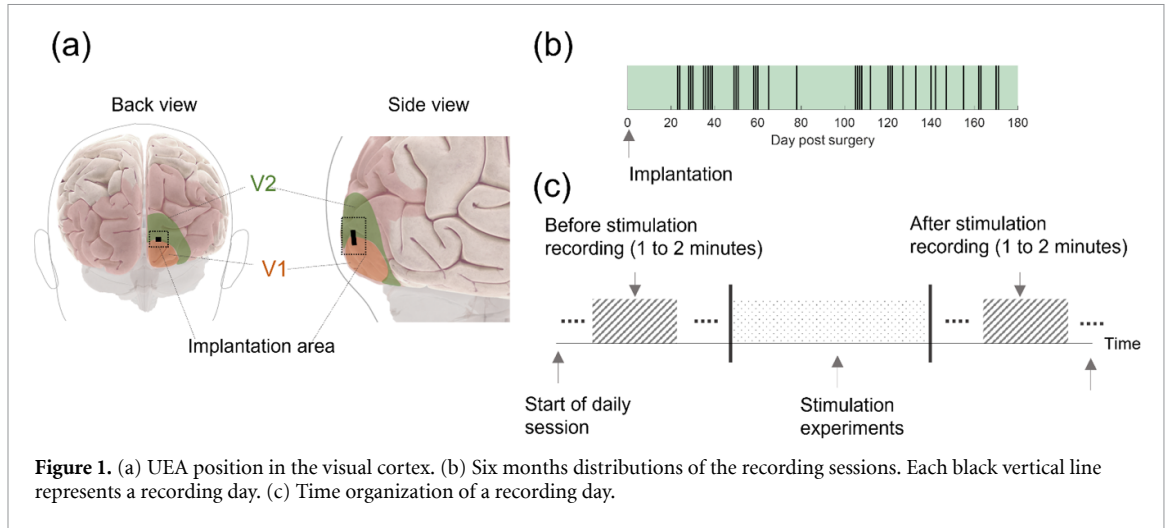


**Figure 1.** (a) UEA position in the visual cortex. (b) Six months distributions of the recording sessions. Each black vertical line represents a recording day. (c) Time organization of a recording day.

became more complex (distinction between shapes, brightness levels, behavioural tasks). The experiments performed and the electrodes used to stimulate changed every day, however, every day each electrode was used to stimulate at least one time during the impedance measurement (1 kHz using the ‘test electrodes’ function of the CereStim 96 multichannel microstimulation system).

Before any analysis, the recordings were segmented to assure that all the signals were lasting 60 s. Then a 2nd order Butterworth filter was used to remove the 50 Hz line noise and all the harmonics up to 400 Hz.

## 2.2. Variance and channel exclusion criteria

For each recording channel, we calculated the voltage variance in 2 s non-overlapping time windows (30 windows for recording lasting 60 s). The variance for each channel on a particular day was then estimated as the mean of the variances among the different windows.

Variance measures the variability of a signal with respect to its mean and can be used to identify the noisy channels. In each recording, we excluded from the analysis the channels that presented a variance bigger than the mean plus three times the standard deviation of the variance of the signals acquired in the first three included days of recording (day post-implantation 23, 24, and 28).

## 2.3. Power spectral density

Power spectral density has been estimated using the Welch method (2 s Hann window, 1 s overlap) [31]. We divided then the spectra into frequencies of interest, in particular from 0.1 to 4 Hz (delta band), from 4 to 8 Hz (theta band), from 8 to 12 Hz (alpha band), from 12 to 30 Hz (beta band), from 30 to 80 Hz (gamma band), from 80 to 200 Hz (high gamma band), from 200 to 400 Hz (very high gamma band), from 400 to 750 Hz, and from 750 to 1500 Hz (multiunit activity band).

## 2.4. Correlation

Correlation is a measure of linear relationships between two signals. It can be evaluated at different time shifts between the signals to highlight the delay between them. Given the signals acquired from two electrodes ( $s_1$  with mean  $\mu_1$  and standard deviation  $\sigma_1$  and  $s_2$  with mean  $\mu_2$  and standard deviation  $\sigma_2$ ) the correlation at different time shifts ( $l$ ) is defined as:

$$\rho_{s_1 s_2}(l) = \begin{cases} \frac{\sum_{n=0}^{N-|l|-1} (s_{1,n+l} - \mu_1)(s_{2,n} - \mu_2)}{\sigma_1 \sigma_2} & l \geq 0 \\ \rho_{s_1 s_2}^*(-l), & l < 0 \end{cases} \quad (1)$$

$\rho_{s_1 s_2}$  assumes values between  $-1$  and  $1$  ( $1$ : signal perfectly correlated  $s_1 = \text{const} \times s_2$ ,  $0$ : no correlation between  $s_1$  and  $s_2$ ,  $-1$ : signal perfectly anticorrelated  $s_1 = -\text{const} \times s_2$ ).

After downsampling each recording to 1 kHz, we calculated the correlation between all possible combinations of electrodes at time shift  $l$  spanning from  $-2$  s to  $+2$  s (1 ms step). These calculations were performed in 2 s non-overlapping windows, which were subsequently averaged to give a more precise estimate of the correlation between two electrodes.

## 2.5. Magnitude of coherence

The magnitude of coherence (also referred to as coherence for simplicity in the following) is a measure of the linear relationship between signals at different frequencies. For two signals  $s_1$  and  $s_2$  it can be evaluated at the frequency  $f$  as:

$$C_{s_1 s_2}(f) = \frac{|S_{s_1 s_2}(f)|^2}{|S_{s_1 s_1}(f)| |S_{s_2 s_2}(f)|} \quad (2)$$

where  $S_{s_1 s_1}(f)$  and  $S_{s_2 s_2}(f)$  are the power spectra density of  $s_1$  and  $s_2$  respectively, and  $S_{s_1 s_2}(f)$  is the cross-spectrum between  $s_1$  and  $s_2$ .  $C_{s_1 s_2}(f) = 0$  when  $s_1$  and  $s_2$  are not correlated at frequency  $f$ ,  $C_{s_1 s_2}(f) = 1$ , when a linear relation between  $s_1$  and  $s_2$  at frequency  $f$  exists.

We calculated the magnitude of coherence between each possible combination of electrodes using the Welch method to estimate the power spectral density (2 s Hann window, 1 s overlap). We averaged then the magnitude of coherence inside the frequency bands already defined for the power spectral density (from delta to very high gamma).

## 2.6. Phase coherence

After having explored the relationship between signals in terms of time (correlation) and frequency (coherence), we evaluated the signal phase relationship using the phase coherence [32]:

$$R = \left| \frac{1}{N} \sum_{k=1}^N e^{i(\phi_{s_1}(t_k) - \phi_{s_2}(t_k))} \right| \quad (3)$$

where  $\phi_{s_1}(t_k)$  and  $\phi_{s_2}(t_k)$  are the phases at time  $t_k$  of the signals  $s_1$  and  $s_2$  respectively.

In order to calculate the instantaneous phase of a signal  $s(t)$ , we calculated its Hilbert transform  $\widetilde{s}(t)$ , and we used the following formula [33]:

$$\phi(t) = \arctan \left( \frac{\widetilde{s}(t)}{s(t)} \right). \quad (4)$$

If the phase difference between  $s_1$  and  $s_2$  is constant at every time  $t_k$ , the signals are perfectly phase-locked and  $R = 1$ , if instead the phase difference is randomly distributed,  $R = 0$ .

After downsampling each recording to 1 KHz, we calculated the phase coherence between all possible combinations of electrodes. The calculation was performed in 2 s non-overlapping time windows. The resulting phase coherence values were subsequently averaged to give a more precise estimate of the phase coherence between the two signals.

To test the significance of the estimated  $R$ , we repeated the calculation of  $R$  for phase-shifted surrogate data [34]. For each 2 s time window, we created 100 surrogate phase signals by applying a circular time shift (selected randomly in the range 0.5–1 s) to one of the two signals. We then compared real data and surrogate data using the Wilcoxon rank-sum test. Indeed, with a circular shift, the phase relation between the signals is removed and we can assess whether the  $R$  value obtained from the real data, could have been obtained from the phase-surrogate data.

## 2.7. Signal analysis over time

In order to check if a linear trend exists in the signals recorded through the 6 months, we calculated the mean across channels of each characteristic (variance, power spectral density, correlation, coherence, phase coherence) for each recording day using the data before and after stimulation separately. We then fitted a line through the average across channels of each characteristic along the 6 months and we tested

if the slope of the line was significantly different from 0 (Wald test).

For correlation, coherence, and phase coherence we checked if the linear trend was different at different electrode distances, by averaging in each day only the channels at a certain distance. Moreover, we checked the influence of different time lags in the 6 months trend of correlation, and the influence of the frequency bands in the 6 months trend of coherence.

## 2.8. Signal evaluation before and after stimulation

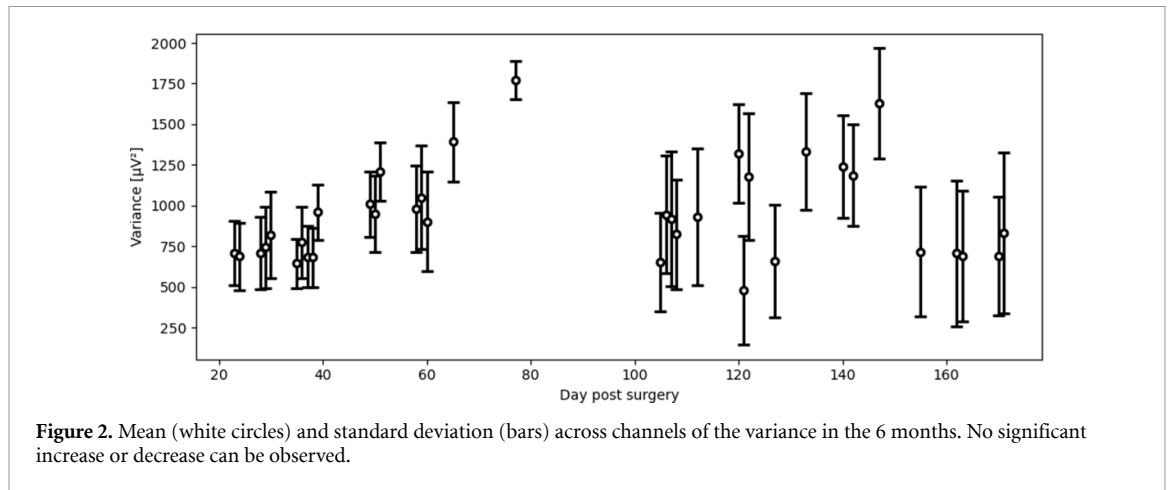
For each recording day, we divided the characteristics extracted from recordings before and after the stimulation grouping together all the channels for variance and power spectral density and all the channel pairs at 0.4 mm distance for correlation, coherence, and phase coherence. We then checked if the data before and after stimulation were significantly different using the Paired  $t$ -test (if the groups' distributions were normal) or the Wilcoxon signed-rank test (if the groups' distributions were not normal). The normality of the data was tested using the Kolmogorov–Smirnov test. For the correlation, we checked the differences between before and after stimulation at different time lags, for the power spectral density and the coherence we checked it in the different frequency bands. In case the statistical test resulted in a significant difference between before and after stimulation, we checked if this was related to an increase or a decrease of the characteristic and if this change was consistent among the recording days.

## 3. Results

### 3.1. Variance stability and electrode selection

Figure 2 shows the mean and standard deviation of the voltage variance across channels on the different recordings before stimulation. No significant increase or decrease of mean variance was observed (average = 912  $\mu$ V,  $p = 0.23$ ) along the 6 months; showing, therefore, good stability of the recorded signals in time, which represents an important factor for the development of any long-term application based on arrays of penetrating electrodes. Although a linear trend is not present in the overall 6 months, figure 2 shows that the variance is constant till day 40, then it is constant between day 50 and day 65 (but higher than in the first days), and again it does not show trends from day 100 to the end.

The number of channels that had to be excluded from the analysis due to variance bigger than the mean plus three times the standard deviation of the variance in the first 3 d of recordings, were on average 11 (range from 0 to 76). None of the channels had to be consistently excluded, meaning that none of the electrodes failed over the whole 6 months period and that all electrodes were able to reliably record high-quality LFPs.



### 3.2. Power spectral density trend

Figure 3(a) reports the power spectral density obtained with the recording before stimulation 107 and 162 d after implantation. The power trend in the 6 months for each frequency band is depicted in figure 3(b). On each day the mean and standard deviation of the power spectral density across all channels is shown.

The slope of the line fitted on the channel's averages power in the 6 months gives a value significantly different from 0 only in the frequency bands 30–80 Hz ( $p = 0.04$ ,  $r = 0.35$ ), and 750–1500 Hz ( $p = 0.0006$ ,  $r = -0.56$ ).

Even with a slope significantly different from 0, the line fit in the 30–80 Hz bandwidth has a very low  $|r|$  value (Pearson correlation coefficient), meaning that there is not a strong linear relationship between the implant days and the power in these bandwidths. The  $|r|$  value in the 750–1500 Hz band instead is higher, confirming a linear decrease of the power in this bandwidth with time. The same decrease at very high frequency was observed in the signal collected with a Utah array in the motor cortex of monkeys and might be related to a decrease in the number of detected spike units [28].

The power spectral density in some frequency bands significantly change up to 40 d post-surgery: it decreases in 1–4 Hz ( $p = 0.017$ ,  $r = -0.724$ ), and it increases in 8–12 Hz ( $p = 0.0002$ ,  $r = 0.92$ ), 12–30 Hz ( $p = 7.78 \times 10^{-7}$ ,  $r = 0.979$ ), and 30–80 Hz ( $p = 0.024$ ,  $r = 0.70$ ). After day 40 post-surgery the only significant change in power spectral density is the decrease in the 750–1500 Hz bandwidth, while no significant change can be seen in all the others frequency bands. All the significant line fits are depicted in figure 3(b) as blue lines.

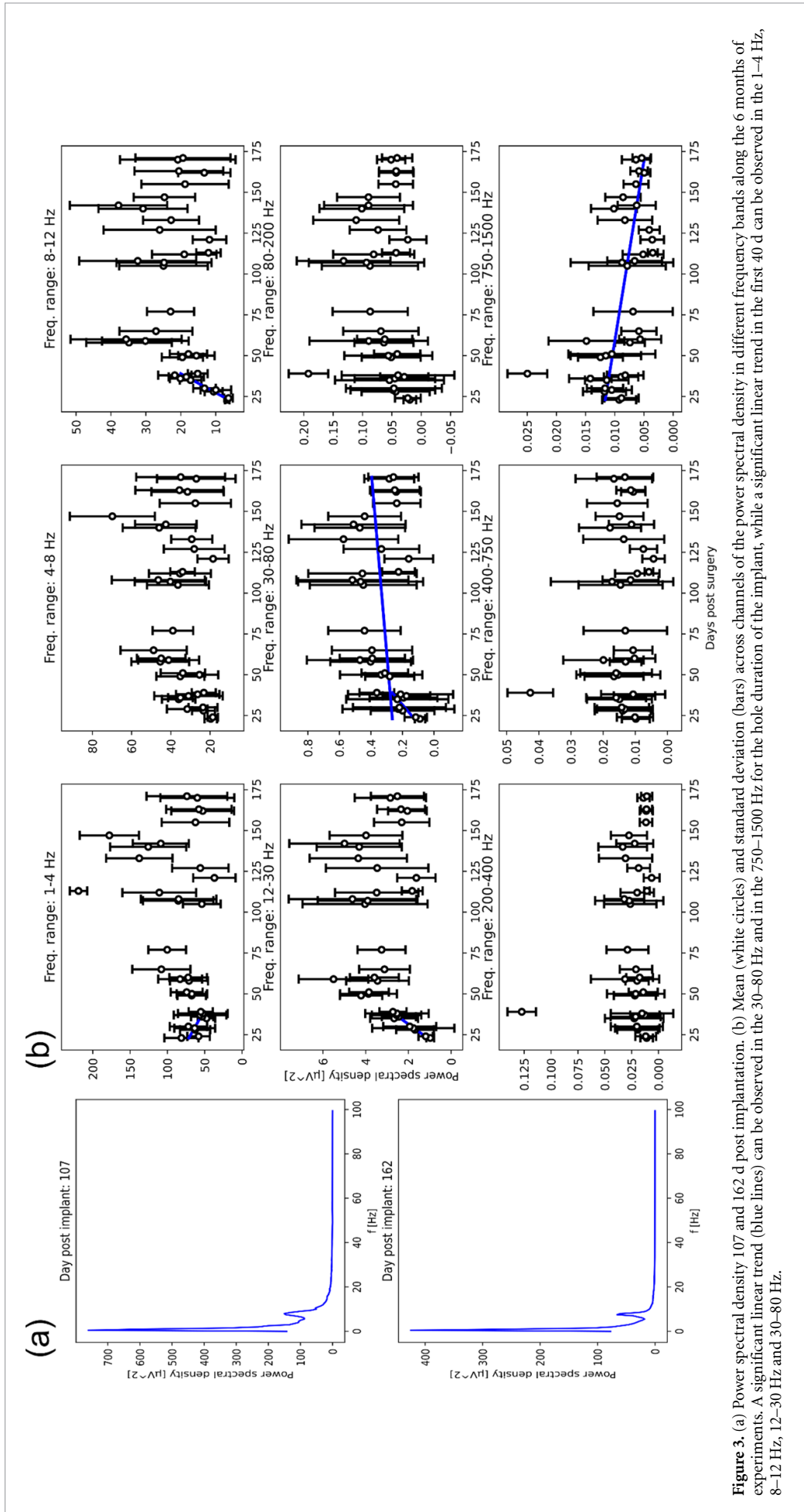
### 3.3. Correlation trend

Figure 4 shows the results obtained with correlations using the data before stimulation. The trend in

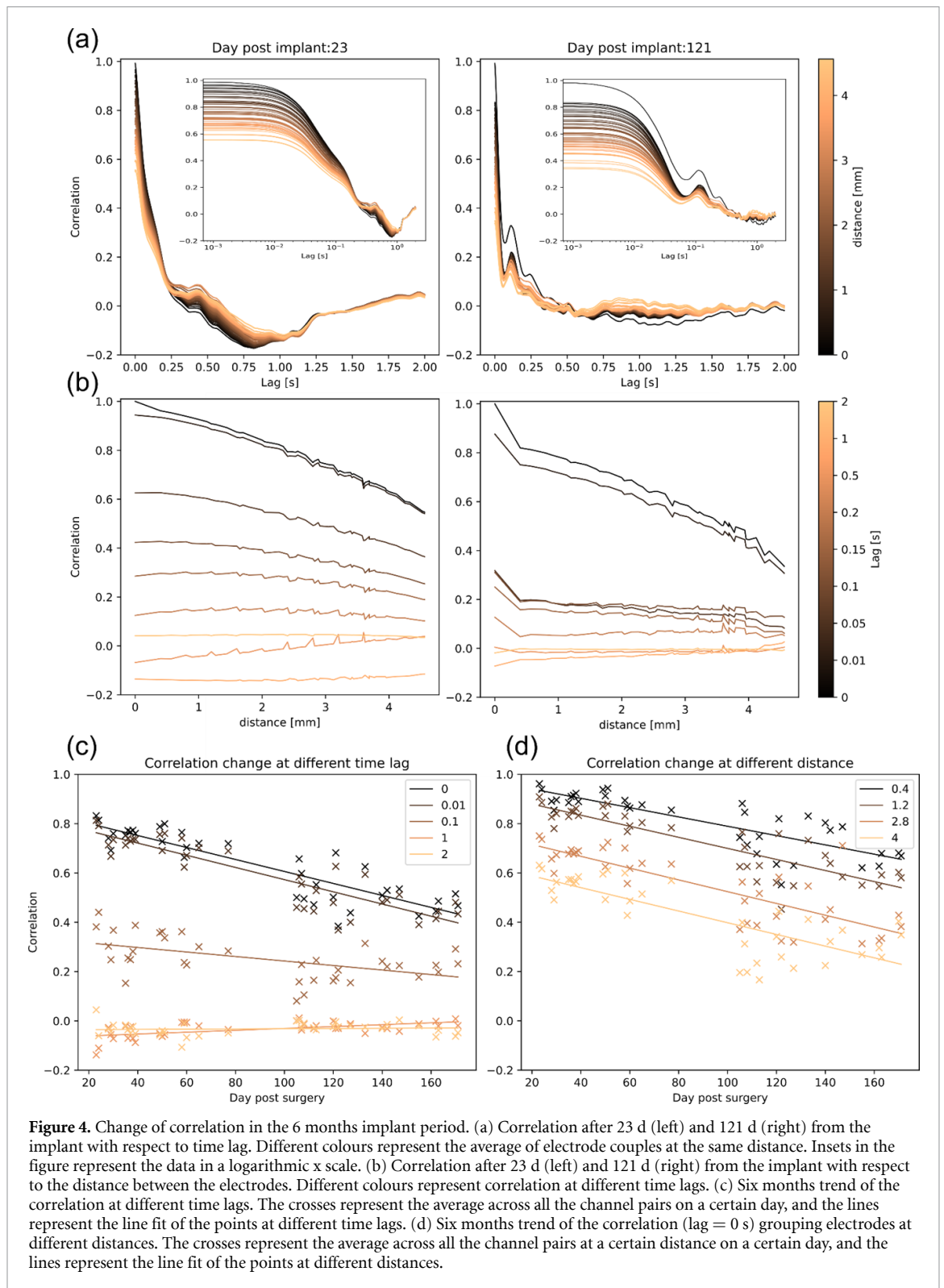
a single recording day with respect to time lag and distance is very similar to the one obtained with a Utah array inserted in the human motor cortex [29]. In particular, the correlation decreases rapidly with the increase of time lag and distance between the electrodes.

Figure 4(a) shows the average correlation at different distances with respect to time lag after 23 d from the implantation day (left) and after 121 d from the implantation day (right). The decrease in correlation with time lag is sharper after 121 d (correlation = 0.5 at 0.03 s of time lag), with respect to 23 d post-surgery (correlation = 0.5 at 0.1 s of time lag).

Figure 4(b) shows the correlation at different time lags with respect to the distance between the electrodes after 23 d from the implant (left) and after 121 d from the implant (right). The decrease in correlation with distance is bigger after 121 d (correlation = 0.5 at 3.5 mm of distance for time lag = 0.01 s), with respect to 23 d post-surgery (correlation >0.5 even at the biggest distance between electrodes for time lag = 0.01 s). The effect of distance between the electrodes can be seen spatially in the electrode array in supplementary figure 1. The highest correlation values (yellow in the figure) are for the electrodes located close to each other. The same spatial organization can be seen at 23 and 121 d post-surgery, but the correlation values decrease faster as we move further away from the electrodes after 121 d. The decrease in correlation shown between day 23 and day 121, can be generalized to all the recording days. Figure 4(c) shows that the average correlation decreases for time-lags smaller than 0.1 s during the 6 months, figure 4(d) shows that the decrease in correlation in the 6 months is independent of the electrode distance considered. Significance, statistics, and slopes of the line fits shown in figures 4(c) and (d) can be found in table 1. The same results have been obtained using after-stimulation recordings (supplementary figure 3).



**Figure 3.** (a) Power spectral density 107 and 162 d post implantation. (b) Mean (white circles) and standard deviation (bars) of the power spectral density in different frequency bands along the 6 months of experiments. A significant linear trend (blue lines) can be observed in the 30–80 Hz and in the 750–1500 Hz for the hole duration of the implant, while a significant linear trend in the 1–4 Hz, 8–12 Hz, 12–30 Hz and 30–80 Hz.



### 3.4. Magnitude of coherence trend

Figure 5 shows the results obtained for the analysis of the magnitude of coherence in the 6 months duration of the implant using before stimulation recordings. Also in this case the results are very similar to the ones shown for the UEAs inserted in the human motor cortex in [29].

Figure 5(a) shows the change of coherence with frequency at different electrodes' distances. The peak

of coherence is in the 8–30 Hz band, and then it decreases towards 0 for high frequencies. The trend of coherence with respect to frequency is shown for the data recorded at 23 and 107 d post-implant. The coherence peak is higher on day 23 compared to day 107.

Figure 5(b) shows the coherence in different frequency bands with respect to the distance between the electrodes after 23 d from the implant (left) and after



**Table 1.** Significance of the decrease in correlation in the 6 months.

Lag (s)	<i>P</i> value	<i>R</i> value	Slope (1 d <sup>-1</sup> )
0	$4.62 \times 10^{-13}$	-0.883 26	-0.002 43
0.01	$1.01 \times 10^{-13}$	-0.893 48	-0.002 47
0.1	0.000 656	-0.534 42	-0.000 91
1	0.000 214	0.572 399	0.000 38
2	0.627 217	0.082 536	$4.46 \times 10^{-5}$
Dist. (mm)	<i>P</i> value	<i>R</i> value	Slope (1 d <sup>-1</sup> )
0.4	$5.84 \times 10^{-10}$	-0.818 94	-0.001 89
1.2	$2.68 \times 10^{-12}$	-0.870 13	-0.002 26
2.8	$1.26 \times 10^{-9}$	-0.809 96	-0.002 42
4	$5.58 \times 10^{-9}$	-0.791 21	-0.002 41

107 d from the implant (right). Coherence decreases with the increase in distance between the electrodes. The decrease in coherence with distance is bigger after 107 d (coherence = 0.5 at 2.5 mm of distance in the 12–30 Hz band), with respect to 23 d post-surgery (coherence bigger than 0.5 even at the biggest distance between electrodes in the 12–30 Hz band). The effect of distance between the electrodes can be seen spatially in the electrode array shown in supplementary figure 1. The highest coherence values (yellow in the figure) are for the electrodes closer to each other. The same spatial organization can be seen in 23 and 107 d post-surgery, but the coherence values get smaller after 107 d getting further away from the electrodes.

The general trend of coherence in the 6 months can be seen in figure 5(c) (average across channel pairs in different frequency bands) and figure 5(d) (average across channels at the same distance in the 8–12 Hz frequency band). A significant decrease in the coherence can be observed for the frequency up to 80 Hz, and this decrease happens independently from the distance between the electrodes included in the average. Table 2 reports the significance and the slope of the linear fit that describes the change of coherence in the 6 months shown in figures 5(c) and (d). The same results have been obtained using after-stimulation recordings (supplementary figure 4).

### 3.5. Phase coherence trend

The average phase coherence among channels is equal to 0.75 after 23 d from the implant, and it is equal to 0.57 after 107 d (figure 6(a), before stimulation recordings). In both cases, the phase coherence extracted from the signals is significantly bigger than the one extracted from the surrogate data ( $p < 0.001$  both 23 and 107 d post-implant). Figure 6(b) shows that the phase coherence decreases with the increase of the distance between the electrodes, reaching smaller values for the recording acquired 107 d post-implant with respect to 23 d post-implant. The spatial distribution of phase coherence in the Utah array can

be seen in supplementary figure 1. The highest phase coherence values (yellow in the figure) are for the electrodes close to each other. The same spatial organization can be seen in 23 and 107 d post-surgery, but the phase coherence values get smaller after 107 d getting further away from the electrodes.

The decrease in phase coherence between day 23 and day 107 post-implant can be generalized to the 6 months. Figure 6(c) shows the phase coherence decrease in the 6 months, while figure 6(d) shows the decrease for electrodes grouped according to the distance. The significance and slope of the phase coherence decrease can be found in table 3. The same results have been obtained using after-stimulation recordings (supplementary figure 5).

### 3.6. Changes induced by the stimulation

We compared the variance, power spectral density, correlation, coherence, and phase coherence between the signals acquired before and after the stimulation each day. The analysis included a total of 26 recording days in which less than 30 channels were excluded by the variance criteria. Figure 7 shows the comparison between before and after stimulation for each characteristic extracted 30 d post-implantation. The significance of the difference and the number of values included in the comparison are reported in table 4 (*N* and *P*-value columns). Although showing significant differences for the day shown, many of the characteristics do not show a consistent increase (or decrease) in all the recording days. The column *number increase/decrease/equal* in table 4, reports how many recording days each characteristic was increasing/decreasing or remaining the same after stimulation.

Variance and power spectral density do not show a consistent increase or decrease after stimulation. Only the power spectral density in the 4–8 Hz bandwidth is consistently increasing (20 out of 26 d). Instead, we can observe a consistent increase in the synchronization measures and in particular in the correlation up to 0.01 s lag (0 s lag, 22 out of 26 d, 0.01 s lag, 21 out

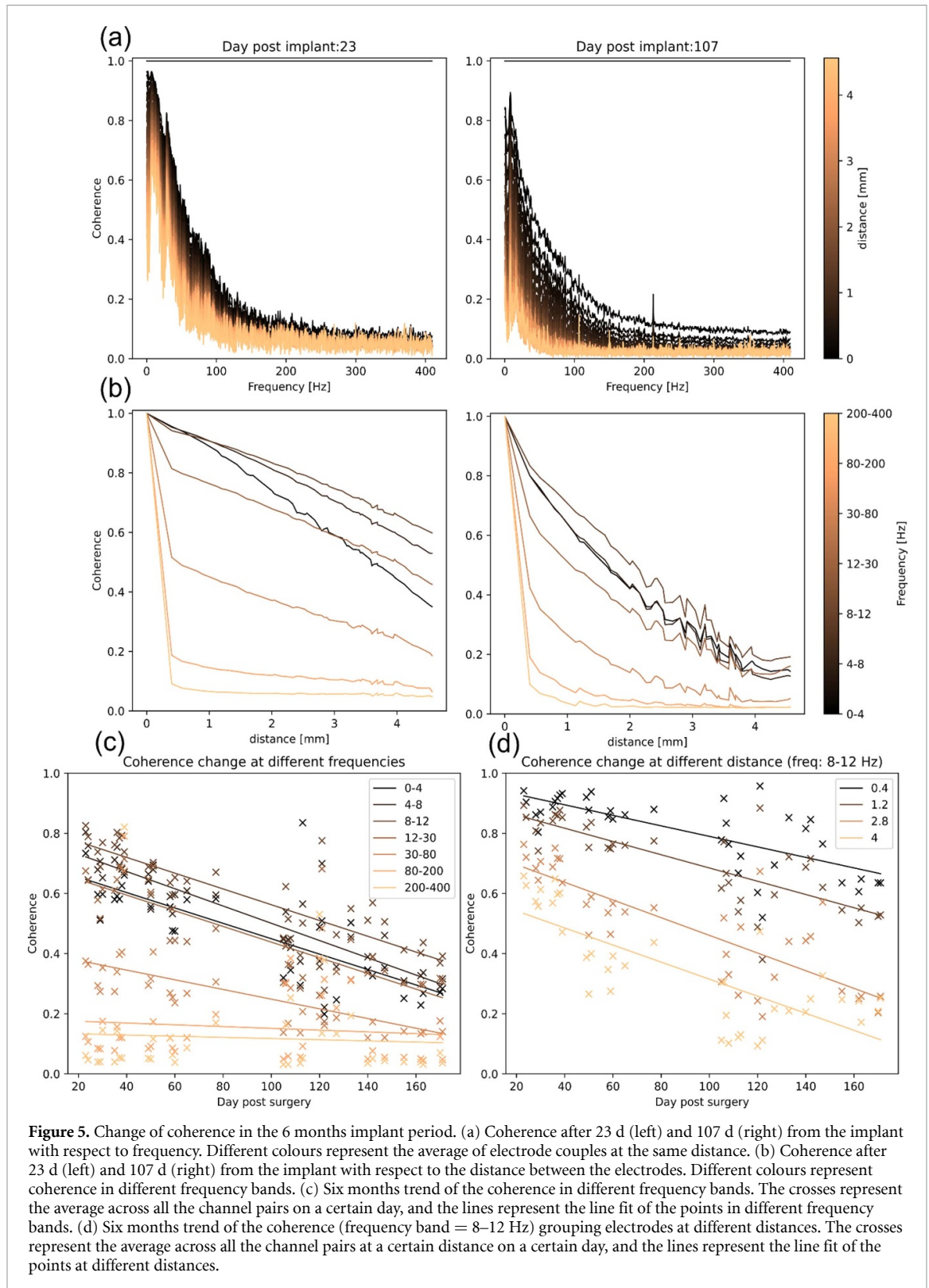


**Figure 5.** Change of coherence in the 6 months implant period. (a) Coherence after 23 d (left) and 107 d (right) from the implant with respect to frequency. Different colours represent the average of electrode couples at the same distance. (b) Coherence after 23 d (left) and 107 d (right) from the implant with respect to the distance between the electrodes. Different colours represent coherence in different frequency bands. (c) Six months trend of the coherence in different frequency bands. The crosses represent the average across all the channel pairs on a certain day, and the lines represent the line fit of the points in different frequency bands. (d) Six months trend of the coherence (frequency band = 8–12 Hz) grouping electrodes at different distances. The crosses represent the average across all the channel pairs at a certain distance on a certain day, and the lines represent the line fit of the points at different distances.

of 26 d), in the coherence up to 80 Hz (1–4 Hz, 22 out of 26 d, 4–8 Hz, 22 out of 26 d, 8–12 Hz, 24 out of 26 d, 12–30 Hz, 24 out of 26 d, 30–80 Hz, 22 out of 26 d), and in the phase coherence (23 out of 26 d).

We then studied this increase in network synchronization over the 6 months (figure 8). The decreasing trend observed for correlation, coherence, and phase coherence in the 6 months for before

stimulation recordings (continuous lines), is present also for after stimulation recordings (dashed lines). However, the figure shows that the line fits obtained from after stimulation recordings (dashed lines) are higher than the ones obtained with before stimulation recordings (continuous lines) for correlation up to 0.01 s of time lag (figure 8(a)), coherence up to 80 Hz (figure 8(b)), and phase coherence (figure 8(c)).

**Table 2.** Significance of coherence decrease in the 6 months.

Freq. (Hz)	<i>P</i> value	<i>R</i> value	Slope (1 d <sup>-1</sup> )
<4	$2.11 \times 10^{-8}$	-0.772 68	-0.002 56
4–8	$4.80 \times 10^{-13}$	-0.882 99	-0.002 87
8–12	$1.47 \times 10^{-10}$	-0.8339	-0.002 62
12–30	$1.25 \times 10^{-9}$	-0.810 13	-0.002 61
30–80	$7.07 \times 10^{-6}$	-0.6652	-0.001 61
80–200	0.554 462	-0.100 37	-0.000 29
200–400	0.719 737	-0.061 03	-0.0002
Dist. (mm)	<i>P</i> value	<i>R</i> value	Slope (1 d <sup>-1</sup> )
0.4	$3.72 \times 10^{-7}$	-0.725 76	-0.001 75
1.2	$5.31 \times 10^{-9}$	-0.791 88	-0.0022
2.8	$9.87 \times 10^{-10}$	-0.812 88	-0.002 94
4	$2.04 \times 10^{-8}$	-0.773 13	-0.002 84

Therefore, the increase in network synchronization shown in figure 7 is independent of the day in which it was evaluated.

The spatial distribution in the UEA of correlation, coherence, and phase coherence 58 d post-implant is shown in supplementary figure 2, distinguishing between signals acquired before and after the stimulation. The highest network synchronization values (yellow in the figure) are for the electrodes close to each other both before and after stimulation. The stimulation, therefore, does not affect the spatial synchronization. However, the results show that after stimulation there is a larger spread of high synchronization values around each electrode (larger yellow area).

#### 4. Discussion

In this work, we showed the trend of LFP signals acquired by a UEA implanted in the visual cortex of a blind subject for a period of 6 months. We showed the signals in terms of variance and power spectral density which represent the energy captured by each single UEA channel, and correlation, coherence, and phase coherence which represent the synchronization and connectivity between channels. Other studies have already shown these measures coming from UEAs implanted in the motor cortex, but using animal models for long-term recordings and human models in intra-surgical recordings [28, 29, 35]. To the best of our knowledge, this is the first time that these measures are shown during a 6 months period in a human and with the electrode positioned in the visual cortex. Moreover, previous studies have used the UEA only for recording purposes, while during this experiment the UEA was used to stimulate the visual cortex [30], opening the possibility to check the effects of intracortical microstimulation in the neural activity reflected by the LFP.

The average variance among channels does not significantly increase or decrease over the 6 months period (figure 2), meaning that the time signals acquired with the UEA are stable over time, thus offering the long-term stability required for a chronically implantable device used to record brain signals in the visual cortex.

Power spectral density significantly decreases during the 6 months period for very high frequencies ( $f > 750$  Hz, figure 3), which are related to neural action potentials. The same reduction in high-frequency components in the signals collected with long-term implanted UEA has been described in monkeys' motor cortex [28] and other studies have reported a decrease in the number of action potentials recorded with chronically implanted electrodes [36, 37]. Therefore, our results in humans are consistent with previous studies on animals.

Frequency components up to 80 Hz show a significant increase or decrease during the first weeks post-implantation but do not show any significant change after this first period. This finding could be related to changes in the electrode–tissue interface following the implantation [38, 39]. One of the consequences of the implantation of UEA in the cortex is the encapsulation of the electrodes in fibrotic tissue which increases the impedance seen by the electrode. The electrode–tissue impedance can be modelled as the parallel between a resistor and a capacitance in series to the impedance of the biological tissue around it [40]. The capacitive component makes that the impedance depends on the frequency, therefore the effect of fibrotic tissue growing around the electrode's tips will affect differently the different frequency bands [41]. The change in power spectral density up to 40 d post-implantation (for frequencies smaller than 80 Hz) could therefore be explained by the growth of some fibrotic tissue around the electrode's tips. In this framework, the mean electrode impedance also increased, particularly during the first 15 d, and

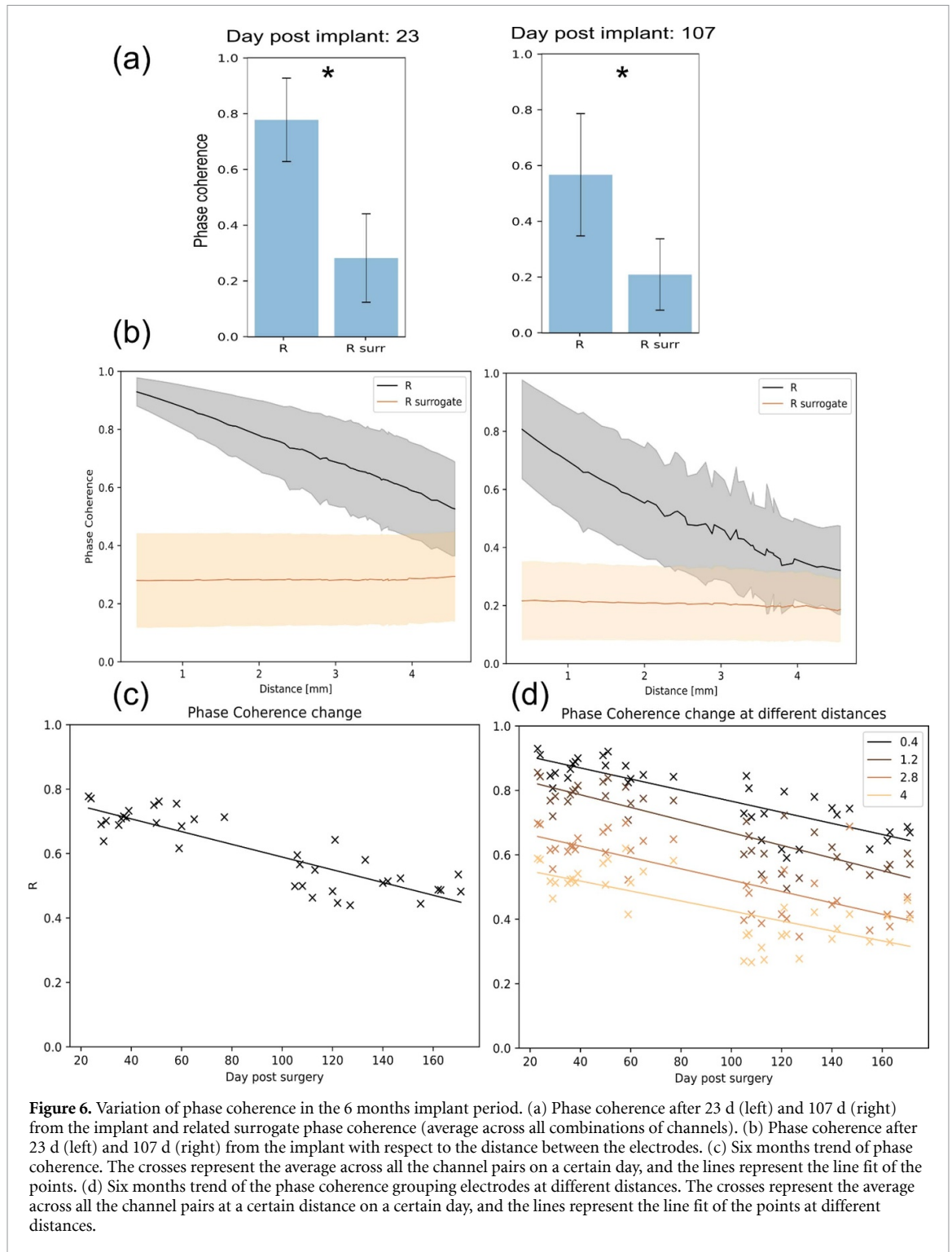


**Figure 6.** Variation of phase coherence in the 6 months implant period. (a) Phase coherence after 23 d (left) and 107 d (right) from the implant and related surrogate phase coherence (average across all combinations of channels). (b) Phase coherence after 23 d (left) and 107 d (right) from the implant with respect to the distance between the electrodes. (c) Six months trend of phase coherence. The crosses represent the average across all the channel pairs on a certain day, and the lines represent the line fit of the points. (d) Six months trend of the phase coherence grouping electrodes at different distances. The crosses represent the average across all the channel pairs at a certain distance on a certain day, and the lines represent the line fit of the points at different distances.

**Table 3.** Significance of phase coherence decrease in the 6 months.

—	<i>P</i> value	<i>R</i> value	Slope ( $1 \text{ d}^{-1}$ )
All	$4.11 \times 10^{-12}$	−0.866 69	−0.001 97
Dist. (mm)	<i>P</i> value	<i>R</i> value	Slope ( $1 \text{ d}^{-1}$ )
0.4	$1.52 \times 10^{-10}$	−0.833 52	−0.001 72
1.2	$2.95 \times 10^{-12}$	−0.869 36	−0.001 96
2.8	$4.21 \times 10^{-8}$	−0.762 26	−0.001 76
4	$6.73 \times 10^{-7}$	−0.714 71	−0.001 55

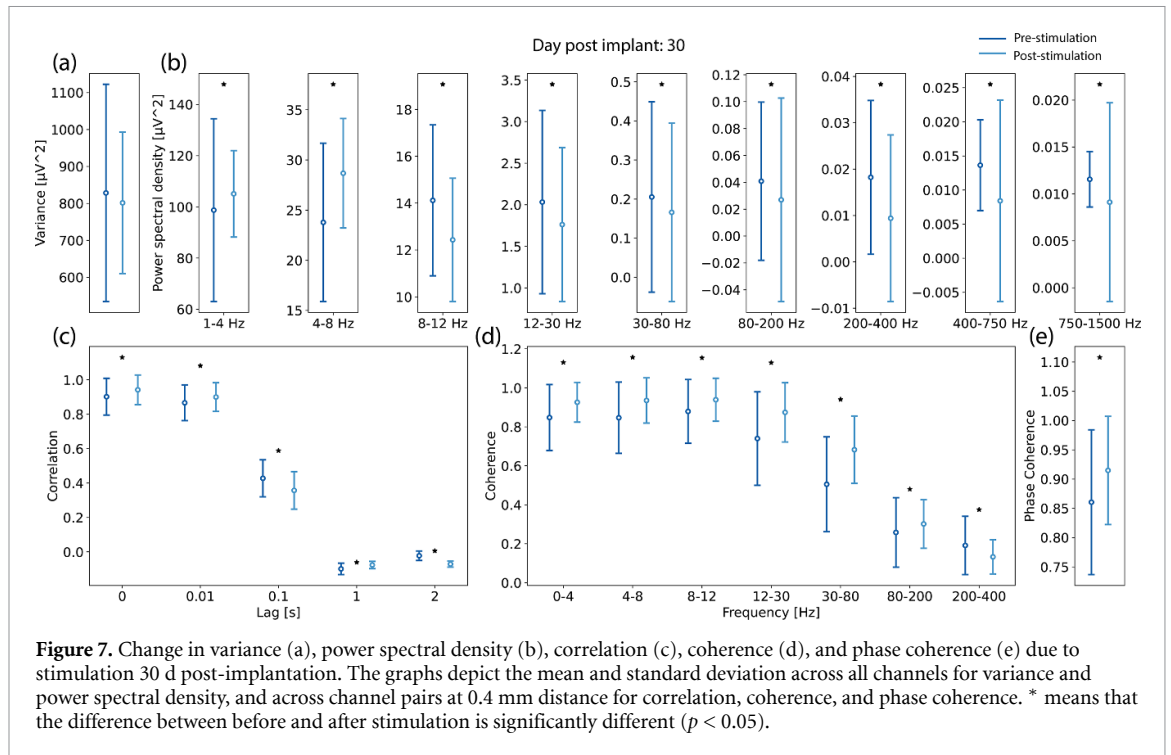


**Table 4.** Difference between pre and post-stimulation recordings. *N* and *P*-value are respectively the number of values included in the comparison and the significance of the difference for the data shown in figure 7 (30 d post-implant). Number of increase/decrease/equal is the number of days in which we measured a significant increase/decrease/no difference of the characteristic post-stimulation with respect to pre-stimulation. The cells highlighted in blue represent a consistent change among days between pre and post-stimulation.

		<i>N</i>	<i>P</i> value	Number increase	Number decrease	Number equal
Variance		91	0.87	12	12	2
Power spectral density	1–4 Hz	91	$6.66 \times 10^{-7}$	11	13	2
	4–8 Hz	91	$6.05 \times 10^{-11}$	20	5	1
	8–12 Hz	91	$4.65 \times 10^{-13}$	16	10	0
	12–30 Hz	91	$4.79 \times 10^{-13}$	15	9	2
	30–80 Hz	91	$2.16 \times 10^{-7}$	6	19	1
	80–200 Hz	91	$4.65 \times 10^{-13}$	4	19	3
	200–400 Hz	91	$4.02 \times 10^{-13}$	5	19	2
	400–750 Hz	91	$1.66 \times 10^{-13}$	7	18	1
	750–1500 Hz	91	$3.92 \times 10^{-14}$	9	15	2
Correlation	0 s	154	$1.33 \times 10^{-11}$	22	2	2
	0.01 s	154	$5.45 \times 10^{-6}$	21	3	2
	0.1 s	154	$6.51 \times 10^{-34}$	11	14	1
	1 s	154	$6.48 \times 10^{-25}$	17	7	2
	2 s	154	$1.90 \times 10^{-26}$	13	12	1
Coherence	1–4 Hz	154	$8.30 \times 10^{-16}$	22	2	2
	4–8 Hz	154	$1.45 \times 10^{-17}$	22	3	1
	8–12 Hz	154	$4.40 \times 10^{-6}$	24	0	2
	12–30 Hz	154	$6.07 \times 10^{-15}$	24	0	2
	30–80 Hz	154	$6.09 \times 10^{-16}$	22	1	3
	80–200 Hz	154	$1.07 \times 10^{-4}$	17	6	3
	200–400 Hz	154	$2.83 \times 10^{-11}$	13	9	4
Phase coherence		154	$2.30 \times 10^{-10}$	23	0	3

then decreased to baseline values starting from 30 to 40 d post-surgery [30], suggesting that the change observed in the power spectral density in the first month could be related to changes in impedances.

Correlation decreases with the increase of time lag in the signals and with the distance between the electrodes (figure 4). The peak of coherence is in the 8–30 Hz frequency band, then it decreases with

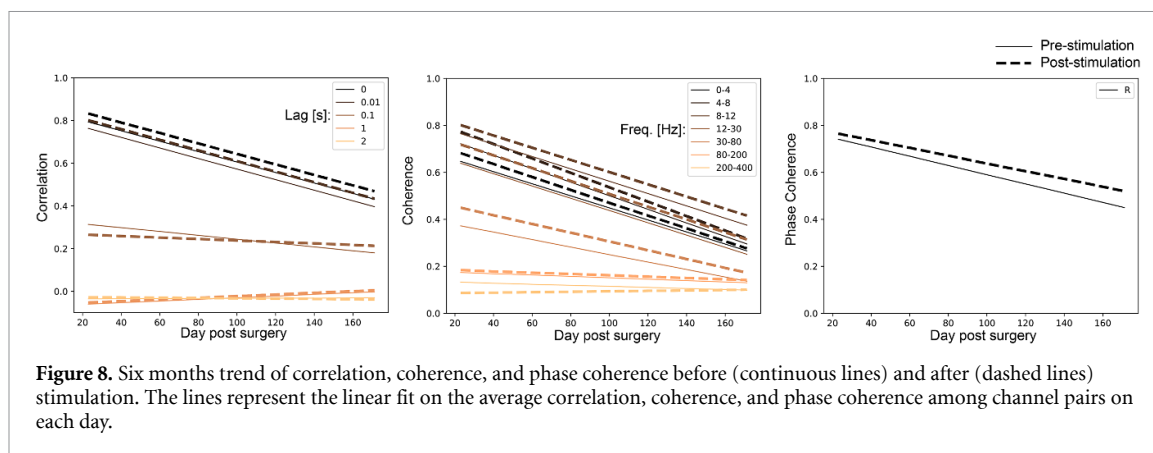


**Figure 8.** Six months trend of correlation, coherence, and phase coherence before (continuous lines) and after (dashed lines) stimulation. The lines represent the linear fit on the average correlation, coherence, and phase coherence among channel pairs on each day.

the increase of the frequency. Coherence and phase coherence also decrease with the distance between the electrodes (figures 5 and 6). These results are similar to the results found in human motor cortex [29]. Therefore, no appreciable difference seems to exist in terms of correlation, coherence, and phase coherence of LFP signals recorded from motor and visual cortex. On the other hand, correlation, coherence, and phase coherence, which are measures of signal synchronization, decreased over the 6 months period, which could reflect adaptive changes of the neural network under the electrode over time [42–44]. Correlation, coherence, and phase coherence could be influenced by the implantation angle of the UEA with respect to the brain surface. Unfortunately, this angle is not known as we could not acquire a magnetic resonance image scan of the UEA inserted in the brain. However, we believe that the synchronization measures are not influenced by this angle as we are not observing two separate regions of synchronization (if the two extremities of the UEA were capturing different cortical layers signals, this could be visible in supplementary figure 1 as a two separate region distribution, instead the distance trend is uniform inside the UEA map).

The second part of the study concerned the comparison of variance, power spectral density, correlation, coherence, and phase coherence before and after stimulation. The variance and power spectral density do not change regularly in the different recording days between before and after stimulation. Therefore, the changes that can be observed in different days are not related to the stimulation. On the other hand, the synchronization between signals acquired by different channels significantly increases after electrical stimulation (figures 7(c)–(e)) and during the 6 months is always higher with respect to before stimulation (figure 8).

One of the study's limitations is that all the data were collected on a single subject. Therefore, we cannot generalize the observed effects and more studies are still needed. During the 6 months of implantation, the participant's medical and

psychological conditions were constantly monitored. The subject was in good health and with the willingness to collaborate in the experiments. Indeed, the performance in executing psychometric experiments remained constant during the 6 months (see figure 3(F) in [30]), and there were no appreciable differences between the performance of the tasks done in the morning or in the afternoon. However, we are planning to measure how fatigue could influence the recorded data through questionnaires to the next participants in the experiment. The kind and duration of experiments and electrical stimulation provided to the participant changed from day to day, making it impossible to correlate the stimulated electrodes with the change in synchronization measures. However, each electrode was used to stimulate at least one time each day during the impedance measurement and the recording procedure for the data used in this analysis is consistent over the 6 months. About 1–2 min of neural data were acquired before stimulation experiments (early morning) and 1–2 min of data were acquired at the end of the daily session (late afternoon).

Neural data are always affected by noise, and particular care has to be taken when drawing conclusions [45]. At the same time, intracortical neural data coming from human subjects are quite difficult to obtain due to the invasiveness of the electrodes. Here, we tried to maintain the data as clean as possible by filtering line noise and always estimating each characteristic as the average on different time windows. We decided to not perform common average re-referencing since this might remove common useful signals among the electrodes. Indeed, re-referencing the signals becomes counterproductive when there is no correlated noise between the reference (or ground) electrode and the recording electrodes [46].

Previous findings [47, 48] report changes in network synchronization after electrical stimulation. Here, we are also observing an increase in synchronization after stimulation and a decrease through the 6 months of implantation. Through the

6 months, the participant learned to distinguish phosphenes induced by the stimulation and started to perform behavioural tasks guided by the induced phosphenes. Hence, the decrease in synchronization happened at the same time as the participant was getting familiar again with light perception. However, the spontaneous activity recorded with the electrodes is not indicative of the participant's behavioural performance in a given task. To do this, it would be necessary to use data from recordings linked to stimulation in a given task, which nowadays, is technically very complex given that the currently available technology greatly limits the acquisition of recordings of neuronal activity in combination with simultaneous electrical stimulation due to the masking generated by the stimulation artefacts.

Although the data are still not enough to conclude that the change in synchronization reflects plastic changes in the neurons surrounding the electrodes due to visual restoration, this could be a reasonable explanation for the synchronization decrease. However, further investigations in more subjects and over a longer period of time are still required.

## 5. Conclusions

Here we report the 6 months trend of LFP signals recorded by a UEA inserted in the visual cortex of a human blind subject. The results obtained are similar to the ones obtained from recordings in animals' and humans' motor cortex, which suggest a substantial similarity in connectivity measures in different brain areas.

Variance and power spectral density in low-frequency bandwidths did not change significantly over the 6 months. This finding suggests that penetrating electrodes such as the UEA could provide the stability required in a clinical device chronically implanted in the visual cortex to stimulate and record brain signals, but further studies are still required. Our results also show that correlation, coherence, and phase coherence of the LFP signals decrease over the 6 months, and increase after stimulation, implying possible changes in the organization of the brain area close to the electrodes in response to electrical stimulation. However, experiments in more subjects and over longer periods of time are still needed to generalize the observed effects.

## Data availability statements

The data that support the findings of this study are available upon reasonable request from the authors. The code used to extract the measures analysed is available at <https://github.com/fabriziograni/Time-stability-and-Connectivity-Analysis-with-Intracortical-signals.git>.

## Acknowledgments


We would like to thank B G and her husband for their extraordinary commitment to this study. This work has been supported in part by Grants RTI2018-098969-B-100 and DTS19/00175 from the Spanish Ministerio de Ciencia Innovación y Universidades, by Grant PROMETEO/2019/119 from the Generalitat Valenciana and by the Bidons Egara Research Chair of the University Miguel Hernández. This project has received funding from the European Union's Horizon 2020 Research and Innovation Programme under the Marie Skłodowska-Curie Grant Agreement No. 861423 (enTRAIN Vision) and No. 899287 (NeuraViPeR). This research was also supported by the group IMED Hospitales and by the John Moran Eye Center of the University of Utah.

## ORCID iDs


Fabrizio Grani  <https://orcid.org/0000-0003-4270-6450>

Cristina Soto-Sanchez  <https://orcid.org/0000-0003-4447-5967>

Fernando Daniel Farfan  <https://orcid.org/0000-0001-8836-7517>

Arantxa Alfaro  <https://orcid.org/0000-0002-5705-8225>

Maria Dolores Grima  <https://orcid.org/0000-0002-0846-8244>

Alfonso Rodil Doblado  <https://orcid.org/0000-0001-8956-3886>

Eduardo Fernández  <https://orcid.org/0000-0002-7052-6011>

## References

- [1] Campbell P K, Jones K E, Huber R J, Horch K W and Normann R A 1991 A silicon-based, three-dimensional neural interface: manufacturing processes for an intracortical electrode array *IEEE Trans. Biomed. Eng.* **38** 758–68
- [2] Normann R A and Fernandez E 2016 Clinical applications of penetrating neural interfaces and Utah electrode array technologies *J. Neural Eng.* **13** 061003
- [3] Alegre-Corté J, Soto-Sánchez C and Fernandez E 2018 Multiscale dynamics of interstimulus interval integration in visual cortex *PLoS One* **13** e0208822
- [4] Bensmaia S J and Miller L E 2014 Restoring sensorimotor function through intracortical interfaces: progress and looming challenges *Nat. Rev. Neurosci.* **15** 313–25
- [5] Simeral J D, Kim S P, Black M J, Donoghue J P and Hochberg L R 2011 Neural control of cursor trajectory and click by a human with tetraplegia 1000 days after implant of an intracortical microelectrode array *J. Neural Eng.* **8** 025027
- [6] Taylor D M, Tillery S I H and Schwartz A B 2002 Direct cortical control of 3D neuroprosthetic devices *Science* **296** 1829–32
- [7] Velliste M, Perel S, Spalding M C, Whitford A S and Schwartz A B 2008 Cortical control of a prosthetic arm for self-feeding *Nature* **453** 1098–101
- [8] Hochberg L R et al 2012 Reach and grasp by people with tetraplegia using a neurally controlled robotic arm *Nature* **485** 372

- [9] Ethier C, Oby E R, Bauman M J and Miller L E 2012 Restoration of grasp following paralysis through brain-controlled stimulation of muscles *Nature* **485** 368–71
- [10] Bouton C E et al 2016 Restoring cortical control of functional movement in a human with quadriplegia *Nature* **533** 247–50
- [11] Moritz C T, Perlmutter S I and Fetz E E 2008 Direct control of paralysed muscles by cortical neurons *Nature* **456** 639–42
- [12] Normann R A, Maynard E M, Guillory K S and Warren D J 1996 Cortical implants for the blind *IEEE Spectr.* **33** 54–59
- [13] Normann R A, Greger B A, House P, Romero S F, Pelayo F and Fernandez E 2009 Toward the development of a cortically based visual neuroprosthesis *J. Neural Eng.* **6** 035001
- [14] Manyakov N V and van Hulle M M 2010 Decoding grating orientation from microelectrode array recordings in monkey cortical area V4 *Int. J. Neural Syst.* **20** 95–108
- [15] Chen X, Wang F, Fernandez E and Roelfsema P R 2020 Shape perception via a high-channel-count neuroprosthesis in monkey visual cortex *Science* **370** 1191–6
- [16] Mitzdorf U 1987 Properties of the evoked potential generators: current source-density analysis of visually evoked potentials in the cat cortex *Int. J. Neurosci.* **33** 33–59
- [17] Mitzdorf U 1985 Current source-density method and application in cat cerebral cortex: investigation of evoked potentials and EEG phenomena *Physiol. Rev.* **65** 37–100
- [18] Buzsáki G, Anastassiou C A and Koch C 2012 The origin of extracellular fields and currents-EEG, ECoG, LFP and spikes *Nat. Rev. Neurosci.* **13** 407–20
- [19] Ray S, Crone N E, Niebur E, Franaszczuk P J and Hsiao S S 2008 Neural correlates of high-gamma oscillations (60–200 Hz) in macaque local field potentials and their potential implications in electrocorticography *J. Neurosci.* **28** 11526–36
- [20] Kahana M J 2006 The cognitive correlates of human brain oscillations *J. Neurosci.* **26** 1669–72
- [21] Diesmann M, Gewaltig M-O and Aertsen A 1999 Stable propagation of synchronous spiking in cortical neural networks *Nature* **402** 529–33
- [22] Narayanan N S and Laubach M 2009 Methods for studying functional interactions among neuronal populations *Methods Mol. Biol.* **489** 135–65
- [23] Jeffreys D A and Axford J G 1972 Source locations of pattern-specific components of human visual evoked potentials. I. Component of striate cortical origin *Exp. Brain Res.* **16** 1–21
- [24] Fallon J B, Irvine D R F and Shepherd R K 2009 Neural prostheses and brain plasticity *J. Neural Eng.* **6** 065008
- [25] Fernández E, Alfaro A and González-López P 2020 Toward long-term communication with the brain in the blind by intracortical stimulation: challenges and future prospects *Front. Neurosci.* **14** 681
- [26] Rajan A T, Boback J L, Dammann J F, Tenore F V, Wester B A, Otto K J, Gaunt R A and Bensmaia S J 2015 The effects of chronic intracortical microstimulation on neural tissue and fine motor behavior *J. Neural Eng.* **12** 066018
- [27] Chen K H, Dammann J F, Boback J L, Tenore F V, Otto K J, Gaunt R A and Bensmaia S J 2014 The effect of chronic intracortical microstimulation on the electrode-tissue interface *J. Neural Eng.* **11** 026004
- [28] Sharma G, Annetta N, Friedenberg D, Blanco T, Vasconcelos D, Shaikhouni A, Rezai A R and Bouton C 2015 Time stability and coherence analysis of multiunit, single-unit and local field potential neuronal signals in chronically implanted brain electrodes *Bioelectron. Med.* **2** 63–71
- [29] Kellis S, Sorensen L, Darvas F, Sayres C, O'Neill K, Brown R B, House P, Ojemann J and Greger B 2016 Multi-scale analysis of neural activity in humans: implications for micro-scale electrocorticography *Clin. Neurophysiol.* **127** 591–601
- [30] Fernández E et al 2021 Visual percepts evoked with an intracortical 96-channel microelectrode array inserted in human occipital cortex *J. Clin. Invest.* **131** 23
- [31] Welch P D 1967 The use of fast Fourier transform for the estimation of power spectra: a method based on time averaging over short, modified periodograms *IEEE Trans. Audio Electroacoust.* **15** 70–73
- [32] Mormann F, Lehnertz K, David P and Elger C E 2000 Mean phase coherence as a measure for phase synchronization and its application to the EEG of epilepsy patients *Phys. D* **144** 358–69
- [33] Rosenblum M and Kurths J 1998 Analysing synchronization phenomena from bivariate data by means of the Hilbert transform *Nonlinear Analysis of Physiological Data* (Berlin: Springer) pp 91–99
- [34] Pereda E, Quiroga R Q and Bhattacharya J 2005 Nonlinear multivariate analysis of neurophysiological signals *Prog. Neurobiol.* **77** 1–37
- [35] Debnath S, Prins N W, Pohlmeier E, Mylavarapu R, Geng S, Sanchez J C and Prasad A 2018 Long-term stability of neural signals from microwire arrays implanted in common marmoset motor cortex and striatum *Biomed. Phys. Eng. Express* **4** 055025
- [36] Freire M A M, Morya E, Faber J, Santos J R, Guimaraes J S, Lemos N A M, Sameshima K, Pereira A, Ribeiro S and Nicolelis M A L 2011 Comprehensive analysis of tissue preservation and recording quality from chronic multielectrode implants *PLoS One* **6** e27554
- [37] Williams J C, Rennaker R L and Kipke D R 1999 Long-term neural recording characteristics of wire microelectrode arrays implanted in cerebral cortex *Brain Res. Protocols* **4** 303–13
- [38] Campbell A and Wu C 2018 Chronically implanted intracranial electrodes: tissue reaction and electrical changes *Micromachines* **9** 430
- [39] Polikov V S, Tresco P A and Reichert W M 2005 Response of brain tissue to chronically implanted neural electrodes *J. Neurosci. Methods* **148** 1–18
- [40] Franks W, Schenker I, Schmutz P and Hierlemann A 2005 Impedance characterization and modeling of electrodes for biomedical applications *IEEE Trans. Biomed. Eng.* **52** 1295–302
- [41] Sillay K A, Rutecki P, Cicora K, Worrell G, Drazkowski J, Shih J J, Sharan A D, Morrell M J, Williams J and Wingeier B 2013 Long-term measurement of impedance in chronically implanted depth and subdural electrodes during responsive neurostimulation in humans *Brain Stimul.* **6** 718–26
- [42] Bola M, Gall C, Moewes C, Fedorov A, Hinrichs H and Sabel B A 2014 Brain functional connectivity network breakdown and restoration in blindness *Neurology* **83** 542–51
- [43] Koenig T, Prichep L, Dierks T, Hubl D, Wahlund L O, John E R and Jelic V 2005 Decreased EEG synchronization in Alzheimer's disease and mild cognitive impairment *Neurobiol. Aging* **26** 165–71
- [44] Xiao R, Shida-Tokeshi J, Vanderbilt D L and Smith B A 2018 Electroencephalography power and coherence changes with age and motor skill development across the first half year of life *PLoS One* **13** 1–17
- [45] Bastos A M and Schoffelen J M 2016 A tutorial review of functional connectivity analysis methods and their interpretational pitfalls *Front. Syst. Neurosci.* **9** 175
- [46] Ludwig K A, Miriani R M, Langhals N B, Joseph M D, Anderson D J and Kipke D R 2009 Using a common average reference to improve cortical neuron recordings from microelectrode arrays *J. Neurophysiol.* **101** 1679–89
- [47] Bloch J A, Khateeb K, Silversmith D B, O'Doherty J E, Sabes P N and Yazdan-Shahmorad A 2019 Cortical stimulation induces network-wide coherence change in non-human primate somatosensory cortex *Proc. Annu. Int. Conf. IEEE Eng. Med. Biol. Soc. EMBS* pp 6446–9
- [48] Krause M R, Zanos T P, Csorba B A, Pilly P K, Choe J, Phillips M E, Datta A and Pack C C 2017 Transcranial direct current stimulation facilitates associative learning and alters functional connectivity in the primate brain *Curr. Biol.* **27** 3086–96.e3